Journal of Animal & Plant Sciences, 35(2): 2025, Page: 470-481
ISSN (print): 1018-7081; ISSN (online): 2309-8694
https://doi.org/10.36899/JAPS.2025.2.0039

IMPACT OF PSEUDOMONAS AERUGINOSA LIPOPOLYSACCHARIDE ON CANDIDA ALBICANS BIOFILM FORMATION AND BLOOD-LABYRINTH BARRIER INTEGRITY IN A RAT MODEL OF SECRETORY OTITIS MEDIA

Y. F. Chen[1,2], D. H. Xie[1,2] and J. Nie[1,2*]

[1]Department of Otorhinolaryngology-Head and Neck Surgery, The Fourth Hospital of Changsha, Changsha 410006, Hunan, China
[2]Department of Otolaryngology Head and Neck Surgery, Affiliated Changsha Hospital of Hunan Normal University, 70 Lushan Road, Changsha, 410006, Hunnan, China.
[*]Corresponding author's Email: niejinchsh@yeah.net

ABSTRACT

The present study aimed to investigate the effect of *Pseudomonas aeruginosa* (PA) lipopolysaccharide (LPS) on *Candida albicans* biofilm formation in a secretory otitis media (SOM) rat model and its potential impact on the integrity of the blood-labyrinth barrier. LPS was extracted from PA standard bacteria, and the effect on the biofilm formation of *Candida albicans* was analyzed. A total of 20 Sprague-Dawley rats were randomly divided into control group (35 μL saline) and SOM group (35 μL PA LPS), with 10 rats in each group. The threshold of auditory brainstem response was measured. The extravasation rate of blood vessels was detected by intravenous injection of Albumin-FITC. Levels of interleukin (IL)-4, IL-6, IL-17, tumor necrosis factor (TNF)-α, and transforming growth factor (TGF)-β in serum were detected. The residual amount of Albumin-FITC and the expression of *ZO-1*, *Occludin*, and *VE-cadherin* were detected in stria vascularis tissues. PA LPS inhibited the biofilm formation of *Candida albicans in vitro*. Compared to control group, the SOM group had a markedly increased brainstem response threshold and lymphedema in the middle ear mucosa ($P \leq 0.05$), the serum IL-4 in SOM group decreased ($P \leq 0.05$), and the levels of IL-6, IL-17, TNF-α, TGF-β, and IFN-γ increased ($P \leq 0.05$). As compared to the control group, the SOM group had an obvious raise in the extravasation rate of vascular Albumin-FITC ($P \leq 0.05$), and residual amount of Albumin-FITC in the stria vascularis ($P \leq 0.05$), and clear reductions in the mRNA expression of *ZO-1* and *Occludin* and the protein expression of *ZO-1*, *Occludin*, and *VE-cadherin* in the stria vascularis ($P \leq 0.05$). PA LPS can inhibit the formation of *Candida albicans* biofilm *in vitro*, PA LPS-induced acute SOM directly disrupts the integrity of the blood-labyrinth barrier by increasing vascular permeability and reducing the expression of barrier proteins such as *ZO-1* and *Occludin*.

Key words: *pseudomonas aeruginosa*; lipopolysaccharide; Biofilm; secretory otitis media; blood labyrinth barrier

Published first online March 01, 2025 Published final April 28, 2025

INTRODUCTION

Secretory otitis media (SOM) is a common cause of hearing loss in children (Pang *et al*., 2020). Eustachian tube dysfunction, bacterial and viral infection, immune response, etc. are the main causes (Bai *et al*., 2019; Covelli *et al*., 2022; Runge *et al*., 2023). The tight junctions of the blood labyrinth barrier in the stria vascularis of the cochlea form a physical barrier that prevents most blood-derived substances from entering the inner ear and maintains the fluid balance of the inner ear (Delaney *et al*., 2023).

Pseudomonas aeruginosa (PA) is a very common opportunistic pathogen in human body, and leading frequent cause of hospital-acquired bloodstream infection (Cruickshank *et al*., 2024). Infections caused by PA are commonly seen in burn or trauma patients, particularly occurring frequently in the middle ear, cornea, urinary tract, and respiratory tract. PA LPS is not only its primary pathogenic component but also a unique structural component of its cell wall. LPS is toxic and can affect the normal growth and division of host cells. LPS can induces the proliferation of middle ear mucosa, glands, and goblet cells, and increase capillary permeability (Chai *et al*., 2021). Inflammation in the middle ear inflammation caused by LPS can induce lead to the release of endotoxin, potentially resulting in and cause inner ear infection through the oval window and other cochlear infections. This can lead to the disruption of inner ear homeostasis, and in severe cases, it may result in the destruction of the ossicles in the inner ear (Weiss *et al*., 2021). LPS can activate macrophages, promote the release of inflammatory cytokines in tissues,

and regulate immune regulatory mechanisms, thereby causing fever, glucose metabolism disorders, and endotoxic shock (Wang *et al*., 2021). LPS substance released during bacterial death, could cause the proliferation of connective tissue in the middle ear mucosa, increase cell density, promote capillary permeability, and destroy the normal mucosal transport system, leading to its accumulation in the middle ear effusion, thus leading to SOM (Offor *et al*., 2022; Lin *et al*., 2022). In addition, LPS can activate the complement response, promote the release of histamine, 5-hydroxytryptamine and other vasoactive mediators, and chemokines from basophils or mast cells, leading to vasodilation, leukocyte aggregation to the inflammatory site, and promoting phagocytosis and the process of SOM (Yang *et al*., 2022).

It was hypothesized that PA LPS can increase the inflammatory response and capillary permeability in the middle ear mucosa, leading to the accumulation of middle ear effusion, and can directly or indirectly trigger inner ear infection and auditory dysfunction by disrupting the blood-labyrinth barrier. This study extracted LPS and PA to analyze their impact on *Candida albicans* biofilm formation. The focus was on investigating the potential pathological mechanisms of PA LPS in chronic SOM, particularly its destructive effects on inner ear homeostasis and the blood-labyrinth barrier. In contrast to traditional research that centers on the effects of LPS on the middle ear mucosa, this study was the first to explore the mechanism by which LPS enters the cochlea through the oval window, subsequently affecting the structure and function of the inner ear. This lays the foundation for understanding the pathogenesis of LPS-induced SOM.

MATERIALS AND METHODS

Extraction of PA LPS: PA (ATCC9027, China Microbial Strain Collection Center, China) preserved in a -80℃ refrigerator was inoculated into a 5% CO_2 Eppendorf C170 incubator at 37℃ for 18 h. A single strain was inoculated into yeast nitrogen-derived liquid (Sigma Aldrich, USA), incubated at 37℃ for 12 h at 75 rpm/min on a ZXY-48 shaking table (Changzhou Runhua Electric Appliance Co., Ltd., China). After centrifugation, the precipitate was rinsed 3 times by using phosphate buffer solution (PBS, Gibco, USA) at 4,000 rpm/min for 5 min. Formalin at 0.5% (V/V) was used to inactivate the precipitate for 24 h at 4℃. The inactivated PA was prepared as a bacterial suspension adopting distilled water, and an equal volume of 90% analytical pure phenol was added for extraction at 65℃ for 10 min. When the temperature was cooled to about 15℃, the samples were centrifuged at 5,000 rpm/min for 30 min, and the aqueous phase was dialyzed in distilled water at 4℃ for 3 days. LPS was obtained after freeze-drying. The obtained LPS was prepared at 100 mg/mL adopting sterile PBS (pH=7.2), detoxified by heat, and stored at 4℃.

Candida biofilm analysis: *Candida albicans* (ATCC90029, China Microbial Strain Collection Center, China) was routinely cultured and diluted in RPMI-1640 liquid containing (Gibco, USA) 0.001, 0.01, 0.1, 1, 10, and 100 μg/mL PA LPS. The concentration of the bacterial solution was adjusted to 5×10^6 cells/mL by cell counting using a hemocytometer under a microscope. A total of 100 μL of the bacterial solution was added to a sterile 96-well plate and cultured at 37°C for 90 minutes with shaking at 75 rpm. The bacteria were then rinsed three times with PBS to remove non-adherent Candida cells. Subsequently, 200 μL of RPMI-1640 medium containing various concentrations of PA LPS was added to each well. The original culture medium was discarded at 6, 12, 24, and 48 hours of culture, and the plates were rinsed three times with PBS. Finally, 40 μL of methylenetetrazolium salt (Sigma-Aldrich, USA), 2 μL of menadione, and 158 μL of PBS were added to each well, and the plates were incubated in the dark at 37°C for 3 hours. The absorbance of each well was detected at 490 nm adopting a HED-SY96S microplate reader (Xi'an Holder Instrument Co., Ltd., China). After 24 h of culture in RPMI-1640 liquid medium supplemented with 100 μg/mL PA LPS, the morphology of *Candida albicans* was observed under an inverted IX73 microscope (Olympus, Japan).

Animals grouping and treatment: a total of 20 Healthy Sprague-Dawley rats weighing 250-300 g (Kaixue Biotechnology Co., Ltd., China) were selected in this experiment. Approval was obtained from the Animal Experiment Ethics Committee of The Fourth Hospital of Changsha provided ethical approval for the study. All rats had normal auricle reflexes and normal bilateral tympanic membranes under the M525 F50 operating microscope (Leica Microsystems, Germany). The rats were randomly divided into control group and SOM group, with 10 rats in each group.

In the control group, 35 μL normal saline was injected into the middle ear cavity of the right ear without any treatment. The left ear of rats in SOM group was not treated, and 35 μL of PA LPS was injected into the middle ear cavity of the right ear. The rats were anesthetized by intramuscular injection of 1 mg/kg ketamine (Sigma Aldrich, USA) combined with fentanyl (Sigma Aldrich, USA). In the supine position, the neck skin was prepared, and the rats were routinely sterilized. An incision was made along the inner edge of the right mandible, and the auditory bulla was carefully blunt-dissected and exposed. The soft tissue covering the auditory bulla was separated, and the wall of the auditory bulla was exposed. Using a microsampler, 35 μL of normal saline or LPS was gently injected into the middle

ear cavity through the auditory bulla wall. The auditory bulla was gently pierced 2 mm from the perforation to equalize the middle ear cavity pressure during the injection, preventing tympanic membrane rupture. After the injection of the corresponding fluid, the two holes were sealed with bone wax, and the incisions were sutured. The tympanic membrane was observed to make sure that there was no fissure or signs of effusion. Once confirmed, , the operation was completed,, and the rats were housed in separate cages for recovery.

Brainstem response detection: The rats were subjected to general anesthesia 48 h after treatment. The transdermal needle-shaped electrodes of the LH2805 brainstem response instrument (Shanghai Hanfei Medical Equipment Co., Ltd., China), the record electrode was placed in the midline of the calvaria, the reference electrode behind the donor ear, and the zero electrode at the nasal root. The sound stimulation was click, hearing level (dB HL), and the stimulation was delivered through earphones. The stimulation frequency was 10.5 times/s, the bandpass filter was 50-3,000 Hz, the superposition number was 1,000, and the recording duration was 10 ms. The response threshold was detected by the decrement method, which decreased by 5 dB each time.

Enzyme-linked immunosorbent assay (ELISA) for detecting serum inflammatory factors: Following each group's respective treatment, rat abdominal aortic blood was collected 48 hours post-treatment. The blood samples were centrifuged at 3,000 rpm for 10 minutes at 4°C to isolate the serum. Serum samples were then subjected to ELISA according to the manufacturer's instructions using a commercial ELISA kit (Beijing Annoron Biological Technology Co., Ltd., China) to quantify the levels of inflammatory cytokines interleukin (IL)-4, IL-6, IL-17, tumor necrosis factor (TNF)-α, and transforming growth factor (TGF)-β, and interferon-gamma (IFN-γ) in the serum.

Tissue preparation: Following general anesthesia, the hearts of the rats were fixed and rapidly exposed. The rats were perfused with PBS (pH=7.3), and after the perfusion solution was clear, 4% polyformaldehyde (Sigma Aldrich, USA) was adopted for perfusion until the tail of the rat was raised and the whole-body muscles trembled. The cochlear tissue was taken by decapination, and the cochlea was fixed in 4% paraformaldehyde (perfusion from the apex of the cochlea and fix) for 12 h at 4℃. The stria vascularis tissues were separated. Through cleaning with PBS, the tissues were stored in triplicate in the refrigerator at -80℃.

Capillary network permeability detection: Through general anesthesia, a 0.1 mm×0.1 mm rectangular window was opened at the base of the cochlea, and the Albumin-FITC reagent (Xi'an Qiyue Biotechnology Co., Ltd., China) was injected intravenously. The extravasation of extravascular Albumin-FITC was observed under a fluorescence microscope, and the extravasation index was adopted for quantitative calculation. A sample of frozen stria vascularis tissue was homogenized applying a homogenizer. After centrifugation, the supernatant was taken, and the residual fluorescence in stria vascularis tissue was detected by a Varioskan LUX multi-well plate fluorescence analyzer (Thermo Fisher, USA).

Morphological observation of the cochlea: The fixed cochlear tissue was removed, washed three times (2 minutes each time) with PBS, and then placed in decalcification solution overnight. The tissues were subsequently rinsed three times (2 minutes each time) with PBS and dehydrated using a series of alcohol solutions: 70%, 70%, 95%, 95%, and 100%, with each gradient for 30 minutes. The tissues were then soaked in xylene I and xylene II solutions for 30 minutes each, followed by immersion in paraffin solution for 60 minutes to embed the tissues. The KH-Q320 paraffin slicer (Hubei Xiaogan Kuohai Medical Technology Co., Ltd., China) was used to prepare paraffin blocks into 6 μm thick slices, and the sections were baked in an oven at 60℃ for 2 h. The tissue was dewaxed and hydrated by gradient alcohol and xylene, and the morphological changes were observed under a microscope.

Real-time fluorescence quantitative PCR detection: The stria vascularis was fully grounded (low temperature operation). TRIzol reagent (Sigma Aldrich, USA) was adopted to extract the total RNA from the tissue. Through detecting the concentration and purity of the extracted RNA, cDNA was synthesized using the cDNA first strand assay kit (MedChemExpress, China). *GAPDH* gene was used as an internal control to measure the expression levels of *ZO-1* and *Occludin* genes in the tissue based on the instructions of the real-time PCR kit (Beijing Solarbio Technology Co., Ltd., China). *GAPDH* as the reference gene, the relative expression of *ZO-1* and *Occludin* was calculated applying $2^{-\Delta\Delta Ct}$. Based on the gene sequences of *ZO-1*, *Occludin*, and *GAPDH*, the amplification primers for each gene were synthesized by GenScript Biotech (Shanghai) Co., Ltd. The primer sequences for each gene are as follows: *ZO-1*: upstream 5'-CTCGGGCATTATTCGCCTTC-3', downstream 5'-GAGAGGGAAATCGTGCGTGACC-3'; *Occludin*: upstream 5'-ACGGTGCCATAGAATGAGATGTTG -3', downstream 5'-CAGCTAGTTGTTCATTTCTGCACCA -3'; *GAPDH*: upstream 5'-AATGCATCCTGCACCACCAA-3', downstream 5'-GTAGCCATATTCATTGTCA-3'.

Western blotting: The stria vascularis tissues were ground and fully lysed in radioimmunoprecipitation assay lysis buffer (Sigma Aldrich, USA). The mixture was then centrifuged at 1,000 rpm for 30 minutes at low

temperature, and the supernatant was collected for protein concentration analysis. The protein concentration was determined using the bicinchoninic acid (BCA) protein quantification kit (Thermo Fisher, USA) according to the manufacturer's instructions. The stacking gel and separating gel were prepared at the appropriate concentrations, and 20 μL of the extracted sample was loaded into each well. Electrophoresis was performed at 120 V for 1 hour. The proteins were transferred to a polyvinylidene fluoride (PVDF) membrane and blocked in blocking solution having 5% skim milk powder for 15 min. The membranes were washed three times (10 minutes each) with Tris-Buffered Saline containing Tween 20 (TBST), followed by overnight incubation at 4°C with primary antibodies (Abcam, UK). The primary antibodies included rabbit anti-human *ZO-1* antibody (1:1000 dilution), rabbit anti-human *Occludin* antibody (1:500 dilution), rabbit anti-human *VE-cadherin* antibody (1:500 dilution), and rabbit anti-human *GAPDH* antibody (1:2000 dilution). The membranes were washed three times with TBST (10 minutes each), followed by a 2-hour incubation at room temperature with horseradish peroxidase (HRP)-conjugated secondary antibody (Abcam, UK). The secondary antibody used was goat anti-rabbit IgG-HRP (1:2000 dilution). The membranes were subjected to rinsing three times (10 min each) adopting TBST, placed in enhanced chemiluminescence immunoimprinting luminescent reagent (Sigma Aldrich, USA), and incubated in the dark for 5 min. Subsequently, the images were observed in the WD-9413C gel imaging system (Shandong Olabo Medical Equipment Co., Ltd., China), with *GAPDH* as internal reference, and the data were analyzed quantitatively by *Image J*.

Statistical analysis: *SPSS 22.0* was adopted for statistical analysis. All experimental data were expressed as mean±standard deviation ($\bar{x} \pm s$), and *t* test was adopted. The difference was considered statistically significant ($P \leq 0.05$).

RESULTS

Effect of PA endotoxin LPS on *Candida albicans* biofilm: The amount of *Candida albicans* biofilm formation was examined at various concentrations of PA LPS, and the effect on the inhibition rate of *Candida* biofilm formation was analyzed (Figure 1A-C). This research found that at the biofilm adhesion stage (1.5 h), biofilm formation stage (24 h), and biofilm maturation stage (48 h), 100 μg/mL PA LPS had the highest suppression rate on *Candida albicans* biofilm formation, which were 55.88%, 88.24%, and 85.29%, respectively. The effect of 100 μg/mL PA LPS on the morphology of *Candida albicans* biofilm found that the biofilm formed by *Candida albicans* in the untreated group contained more hyphae, and the hyphae were intertwined. However, after 100 μg/mL PA LPS treatment, *Candida albicans* biofilm suggested yeast phase, and only a few hyphae were formed (Figure 1D). The control group had a hyphal count of 12.8±2.1 hyphae per field of view, with a hyphal ratio of 84.5±5.2%. After treatment with 100 μg/mL PA LPS, the hyphal count decreased to 3.4±0.8 hyphae per field of view, and the hyphal ratio decreased to 23.1±3.4% ($P \leq 0.01$). The proportion of *Candida albicans* in the 100 μg/mL PA LPS treatment group was significantly higher than in the control group (76.9±3.3% *vs* 15.5±3.6%) ($P \leq 0.01$).

Hearing and cochlear morphology in rats: The hearing changes of each group of rats are shown in Figure 2A. As against the control group, the brainstem response threshold of the rats was markedly increased following injection of PA LPS into the middle ear cavity ($P \leq 0.01$). The morphological changes in the cochlear tissues of rats were depicted in Figure 2B. In the control group, the structures of the apex, middle, and base turns of the cochlea were all normal, with no evidence of inner lymphatic edema. In the SOM group, rats exhibited mild inner lymphatic edema in the apex, middle, and base turns of the cochlea, while folding was observed at the location of Reissner's membrane, as indicated by the black arrows.

Inflammatory response in rats: The levels of inflammatory cytokines in rat serum were detected using the ELISA method pre- and post-intervention. The baseline levels of IL-4, IL-6, IL-17, TNF-α, TGF-β, and IFN-γ in the control and SOM groups were as follows: (28.2±2.6 pg/mL *vs* 29.1±1.6 pg/mL), (9.8±0.93 pg/mL *vs* 9.2±0.87 pg/mL), (4.3±0.4 pg/mL *vs* 3.9±0.6 pg/mL), (25.6±1.2 pg/mL *vs* 26.1±1.3 pg/mL), (21.3±2.5 pg/mL *vs* 20.4±1.7 pg/mL), and (150.4±13.8 pg/mL *vs* 148.6±12.2 pg/mL). No statistically significant differences were observed in the baseline inflammatory cytokine levels between the control and SOM groups ($P > 0.05$). The inflammatory cytokine levels of the rats in each group after intervention are shown in Figure 3. It was observed that compared to the control group, rats in the SOM group exhibited a significant decrease in IL-4 levels in serum, while IL-6, IL-17, TNF-α, TGF-β, and IFN-γ levels were significantly elevated, with statistically significant differences ($P \leq 0.01$). One-way analysis of variance (ANOVA) was used to compare the cytokine levels between the control and SOM groups. The ANOVA results showed that the levels of IL-4, IL-6, IL-17, TNF-α, TGF-β, and IFN-γ were significantly different between the two groups ($P \leq 0.01$). To further determine the specific nature of the intergroup differences, Tukey's honestly significant difference (HSD) post hoc test was conducted. The results indicated that the IL-4 level in the SOM group was significantly lower than that in the control group ($P \leq 0.01$), while the levels of IL-6, IL-17,

TNF-α, TGF-β, and IFN-γ were significantly higher in the SOM group compared to the control group ($P \leq 0.01$).

Blood labyrinthine barrier in rats: Intravenous injection of Albumin-FITC was employed to assess the permeability of the rat capillary network. In the control group, Albumin-FITC was confined within the blood vessels, whereas in the SOM group, there was a significant increase in vascular permeability, accompanied by the penetration of Albumin-FITC (Figure 4A). The Albumin-FITC extravasation index results are illustrated in Figure 4B, demonstrating a marked increase in Albumin-FITC extravasation in rats from the SOM group compared to the control group, with statistically significant differences (0.36±0.04 *vs* 0.49±0.05) ($P \leq 0.01$). Additionally, the residual amount of Albumin-FITC in the SOM group was notably higher than that in the control group (Figure 4C). Semi-quantitative fluorescence analysis of Albumin-FITC levels in vascular tissues is presented in Figure 4D. It was observed that compared to the control group, rats in the SOM group exhibited a significant increase in residual Albumin-FITC levels (1.15±0.18 *vs* 1.48±0.08), with statistically significant differences ($P \leq 0.01$).

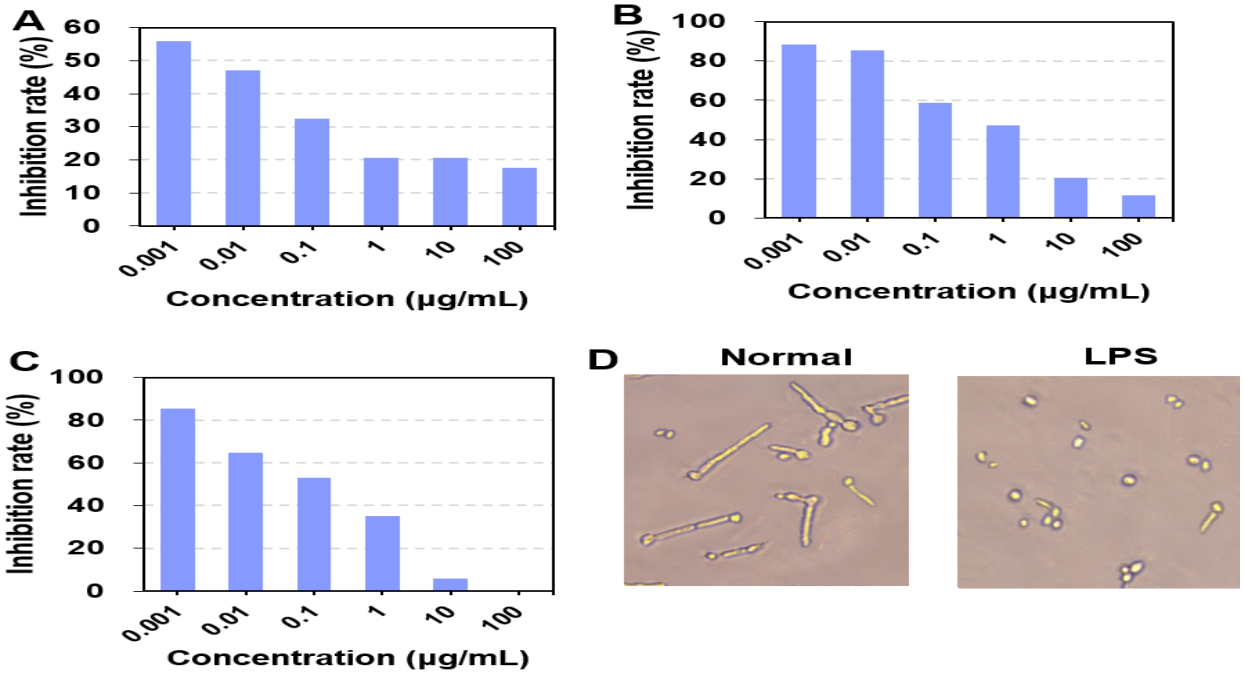

Figure 1. Effect of PA endotoxin LPS on biofilm formation and morphology of *Candida albicans*. A: at biofilm adhesion stage; B: at biofilm formation stage; C: at biofilm maturation stage; D: morphological observation of biofilm after 100 μg/mL PA endotoxin LPS treatment, ×40.

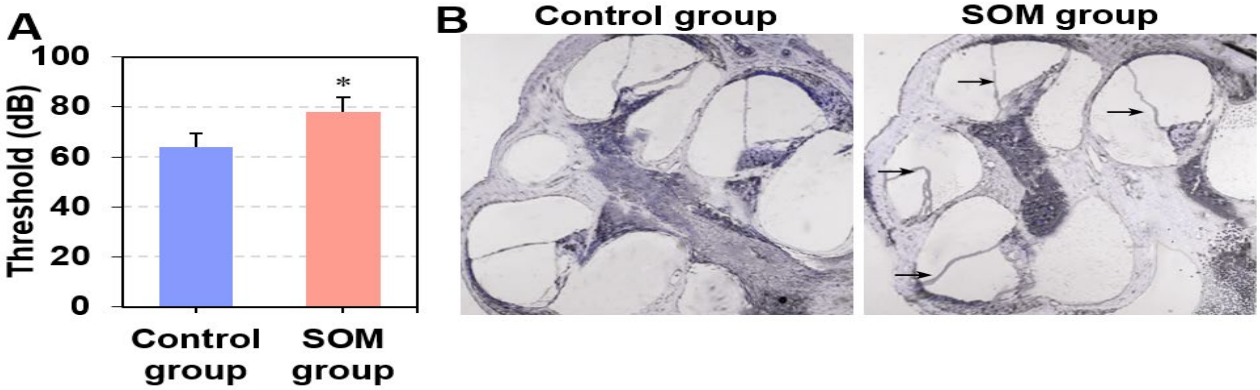

Figure 2. Observation of auditory brainstem response threshold and cochlear morphology in rats. A: threshold detection of auditory brainstem response; B: observation of cochlear morphology (×40). Compared with the control group, $^{*}P \leq 0.01$.

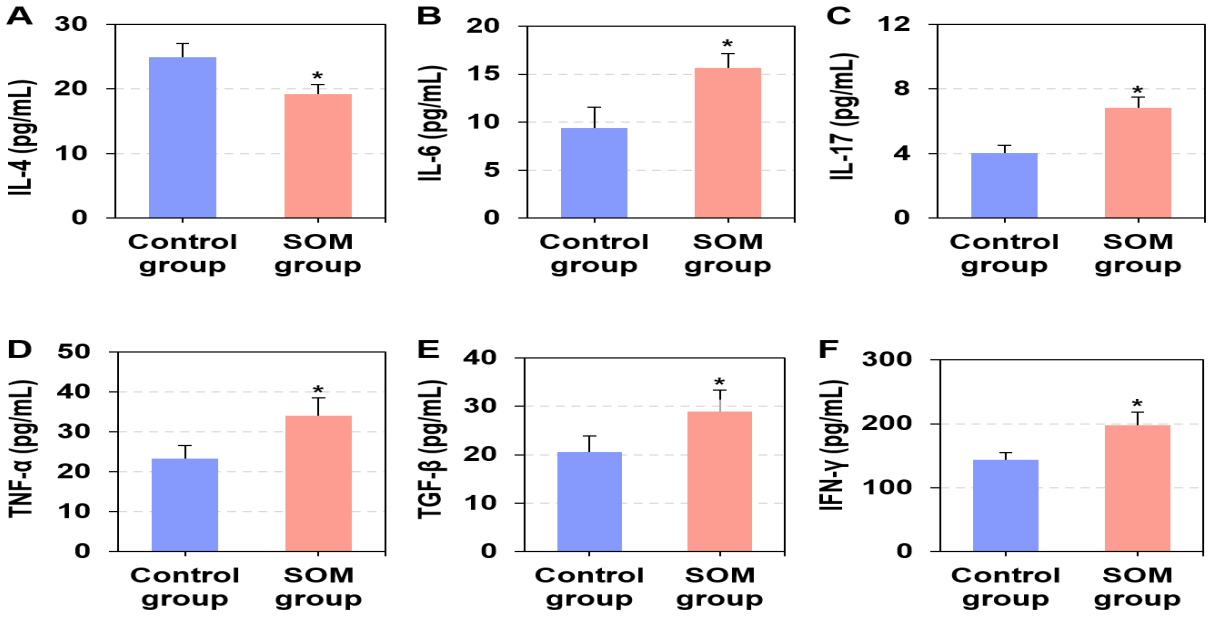

Figure 3. Detection of serum inflammatory factors in rats. A: IL-4 level; B: IL-6 level; C: IL-17 level; D: TNF-α level; E: TGF-β level; F: IFN-γ level. Compared with the control group, *$P \leq 0.01$.

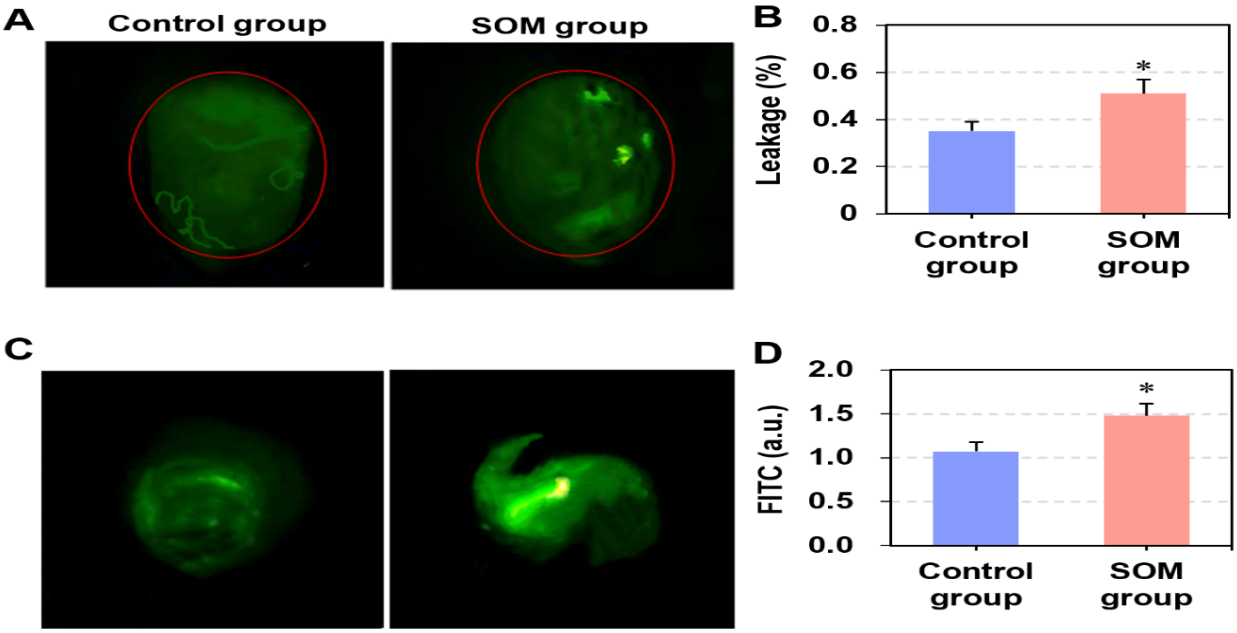

Figure 4. Measurement of blood labyrinth barrier permeability (×400). A: vascular Albumin-FITC assay; B: comparison of Albumin-FITC extravasation rate; C: detection of residual Albumin-FITC fluorescence in stria vascularis; D: quantitative detection of residual Albumin-FITC in the stria vascularis. Compared with control group, *$P \leq 0.05$.

Tight junction protein expression of blood labyrinth barrier: Fluorescence quantitative PCR was utilized to assess the expression levels of *ZO-1* and *Occludin* in vascular tissues. The results, as depicted in Figure 5A and Figure 5B, revealed a significant decrease in the expression levels of *ZO-1* (1.00±0.12 *vs* 0.19±0.08) and *Occludin* (1.00±0.11 *vs* 0.73±0.09) in the vascular tissues of rats from the SOM group compared to the control group, with statistically significant differences ($P \leq 0.01$). Western blot analysis was conducted to examine the protein expression changes of *ZO-1* (1.00±0.10 *vs* 0.61±0.09), *Occludin* (1.00±0.09 *vs* 0.52±0.06), and *VE-cadherin* (1.00±0.10 *vs* 0.59±0.07) in rat vascular tissues. In Figure 5C, Figure 5D, Figure 5E, and Figure 5F, it was

observed that compared to the control group, rats in the SOM group exhibited a notable decrease in the protein expression levels of *ZO-1*, *Occludin*, and *VE-cadherin* in vascular tissues, with statistically significant differences ($P \leq 0.01$).

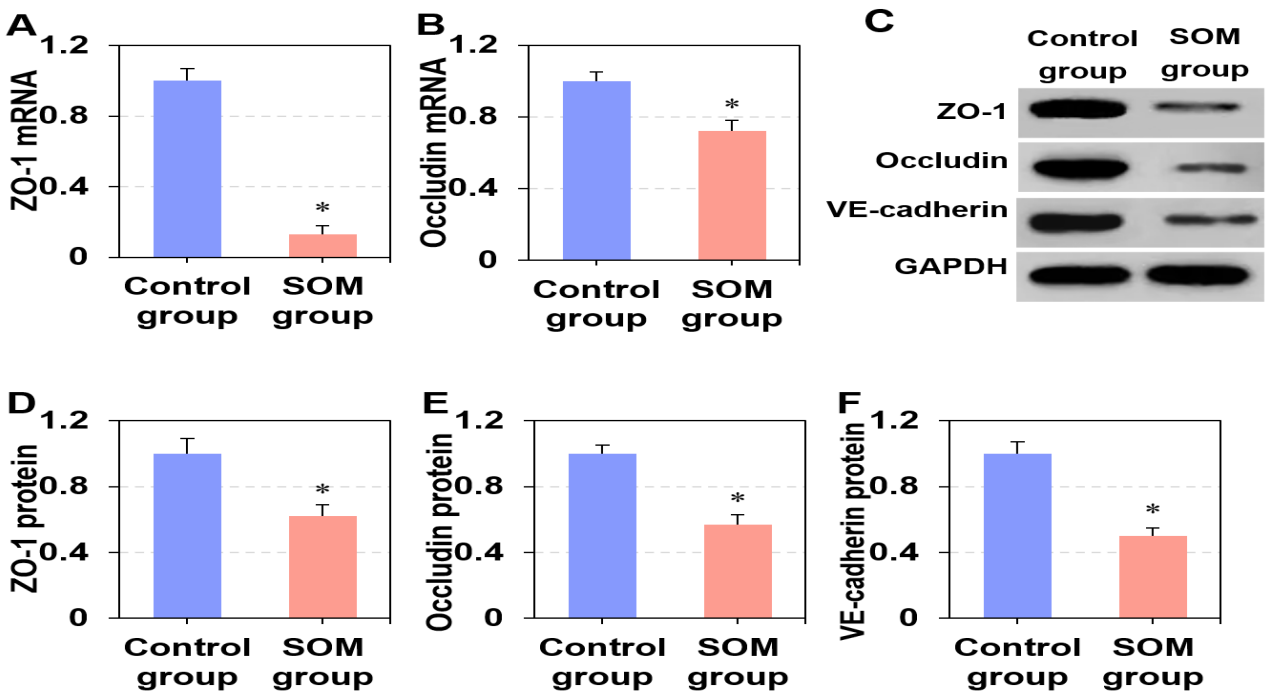

Figure 5. Detection of tight junction protein expression in rat stria vascularis. A: *ZO-1* mRNA expression; B: *Occludin* mRNA expression; C: Western blotting; D: expression of *ZO-1* protein; E: *Occludin* protein expression; F: *VE-cadherin* protein expression. Compared with control group, $^{*}P \leq 0.05$.

DISCUSSION

The formation of bacterial biofilms is a dynamic process, primarily consisting of the reversible attachment and colonization stage, the irreversible attachment and aggregation stage, the biofilm maturation stage, and the bacterial detachment and reattachment stage (Cayetano *et al*., 2022; Li *et al*., 2023; Isom *et al*., 2022). The stages of *Candida albicans* biofilm formation can be divided into the adhesion stage (1-2 hours), formation stage (12-24 hours), and maturation stage (30-72 hours) (Pereira *et al*., 2021). This study found that PA LPS at a concentration of 100 μg/mL exhibited the most significant inhibitory effect on *Candida albicans* biofilm formation. In the three different stages of biofilm formation, the inhibition rates of PA LPS were 55.88%, 88.24%, and 85.29%, respectively. These data suggest that PA LPS not only significantly inhibits the initial adhesion of biofilms but also effectively prevents further biofilm formation and maturation. Morphological analysis showed that after treatment with 100 μg/mL PA LPS, the *Candida albicans* biofilm exhibited a yeast form, with a significant reduction in hyphal count and a marked decrease in the hyphal ratio. These findings suggest that PA LPS not only reduced biofilm formation but also inhibited the formation of hyphae, preventing the transition of *Candida albicans* from the yeast form to the hyphal form. This morphological change further supports the critical role of PA LPS in inhibiting biofilm formation. After PA LPS treatment, the hyphal ratio was significantly lower, indicating that PA LPS may suppress hyphal formation and biofilm development by regulating genes and proteins associated with hyphal growth. The significantly increased proportion of yeast form after PA LPS treatment contrasts sharply with the reduction in hyphal form, suggesting that PA LPS may inhibit the transition from yeast to hyphal form by promoting the yeast form phenotype, thus reducing biofilm formation. This effect could be due to PA LPS disrupting the cell membrane structure of *Candida albicans*, impairing its energy metabolism and signal transduction pathways, thereby inhibiting hyphal formation. Furthermore, PA LPS may modulate host immune responses associated with biofilm formation, weakening the ability of *Candida albicans* to colonize within the biofilm.

Biofilm plays a crucial role in the pathogenesis and progression of SOM. SOM is a non-suppurative inflammatory disease of the middle ear, characterized by middle ear effusion, which is the main clinical feature of SOM (Lechien *et al*., 2021). Immunological responses

and dysfunction of the eustachian tube are currently believed to be potential factors contributing to the onset of SOM (Zhang *et al*., 2021). The presence of endotoxin in the middle ear cavity of SOM patients suggests the significant role of endotoxin in the occurrence and progression of this disease. Induction and establishment of animal models of SOM mainly involve the use of bacteria and their metabolites, cytokines, inflammatory mediators, and immune responses, albeit with complex operational procedures (Zhang *et al*., 2022). LPS plays a crucial role in the progression of SOM by inducing a series of inflammatory reactions within the middle ear cavity, leading to proliferation of middle ear mucosa, glands, and goblet cells, as well as promoting vascular dilation and increased vascular permeability (Kim *et al*., 2022; Hu *et al*., 2021). Brainstem response testing belongs to short-latency evoked potentials and can be used for differential assessment of hearing loss, such as in conductive hearing loss, Meniere's disease, acoustic neuroma, brainstem lesions, and others (Acke *et al*., 2022). In this research, the rat model of SOM was established by intratympanic injection of endotoxin LPS from PA, and brainstem response were measured in the rats. The results revealed a significant increase in brainstem response thresholds in rats following injection of PA LPS into the middle ear cavity compared to the control group. This suggests that injection of PA LPS into the middle ear cavity has a notable impact on the auditory levels of rats, indicating structural changes in the cochlea and providing initial insights into the effects of PA endotoxin LPS on the auditory system. Although the pathogenesis of SOM remains incompletely understood, immune factors play a crucial role in its onset and development. Endotoxin LPS is a bacterial endotoxin that directly damages outer hair cells and induces mucosal edema (Ko *et al*., 2023). Furthermore, studies have shown that endotoxin LPS can lead to insufficient blood supply to the cochlea, where the microcirculation of the cochlear lateral wall is essential for maintaining normal ion channel function (Kaya *et al*., 2019). This research revealed that injection of PA endotoxin LPS may lead to certain abnormal changes in the inner ear structure of rats, including mild inner lymphatic edema and folding of Reissner's membrane. These changes may be associated with the formation of the otitis media model induced by PA endotoxin LPS. Furthermore, the research also found a significant decrease in serum IL-4 levels and a significant increase in IL-6, IL-17, TNF-α, TGF-β, and IFN-γ levels after injection of PA endotoxin LPS in rats. This suggests that the inflammatory response is enhanced in the SOM group rats, which may be associated with the pro-inflammatory effects of PA LPS. LPS is a major component of the P. aeruginosa cell wall and can induce the release of numerous inflammatory cytokines by activating the host's innate immune system. LPS binds to the host's Toll-like receptor 4 (TLR4), initiating downstream signaling pathways, activating transcription factors such as nuclear factor kappa B (NF-κB), and promoting the expression of various pro-inflammatory cytokines (Liu *et al*., 2024). LPS can also suppress the expression of anti-inflammatory cytokines, leading to a weakened anti-inflammatory response and allowing the pro-inflammatory response to dominate (Oliveras-Cañellas *et al*., 2023).

Endotoxin LPS can affect the permeability of the blood-labyrinth barrier, increasing its permeability and inducing vascular leakage (Jiang *et al*., 2019). The spiral ligament (forming the outer wall of the cochlear duct) contains a large amount of tissue with capillary loops and small blood vessels known as the vascular stria, which is the site of lymph formation within the cochlear duct (Bae *et al*., 2021). The vascular stria also contains marginal cells, melanocytes, and endothelial cells. The results demonstrated that compared to the control group, both the extravasation and residual amounts of Albumin-FITC in the SOM group rats were significantly increased. This finding suggests that injection of PA LPS into the middle ear cavity may lead to an increase in vascular permeability in the rat ear tissues, resulting in increased extravasation and retention of Albumin-FITC, a tracer. This phenomenon may be related to the inflammatory response induced by PA endotoxin LPS in the pathogenesis of otitis media.

The basis for the regulation of blood labyrinth barrier permeability lies in the status of intercellular tight junctions, which are composed of transmembrane proteins (such as *Occludin*) and cytoplasmic scaffolding proteins (such as ZO), forming connections with cytoskeletal proteins (Sekulic-Jablanovic *et al*., 2022). Tight junctions serve as paracellular barriers between cells, regulating the transmembrane transport of water, ions, and macromolecules through the paracellular pathway (Gu *et al*., 2022). They are present between cells and play a crucial role in regulating the barrier function of the paracellular pathway. Tight junctions constitute the foundation of the blood labyrinth barrier, forming tight physical barriers that prevent the entry of most blood-borne substances into the inner ear, thus maintaining ion balance in the perilymph and endolymph (Lin *et al*., 2021; Zheng *et al*., 2024). Among the components of tight junctions, *Occludin* binds with adjacent cells on the extracellular side to form paracellular seals, thereby influencing the transmembrane resistance of the blood labyrinth barrier and the formation of intercellular water channels (Glueckert *et al*., 2018). Previous studies have confirmed the expression of tight junction-associated proteins such as *ZO-1*, *Occludin*, and *VE-cadherin* in the blood labyrinth barrier (Sung *et al*., 2023). *ZO-1* is one of the proteins involved in tight junction formation, and its expression loss can affect the stability of tight junction structures, acting as a bridge between *Occludin* and Actin (Haas *et al*., 2022). *Occludin*, as a transmembrane

protein, participates in the composition of tight junctions and also regulates intercellular permeability (Rawat *et al*., 2020). Studies have shown that cerebral ischemia can lead to tyrosine phosphorylation of *Occludin* and a significant decrease in *ZO-1* levels, thereby causing dysfunction of the blood-brain barrier (Du *et al*., 2020). *VE-cadherin* belongs to the adherens junction family and is involved in interendothelial cell communication and extracellular signal transduction. Loss of *VE-cadherin* can affect vascular permeability and promote the release of inflammatory factors (Yang *et al*., 2020). This study demonstrated that in the SOM group, the expression levels of *ZO-1*, *Occludin*, and *VE-cadherin* proteins in the vascular stria tissues of rats were significantly lower than those in the control group. The decreased expression levels of these proteins can lead to increased vascular permeability, making the blood vessels more susceptible to leakage due to external factors. This finding is consistent with the previously observed increase in extravasation and retention of Albumin-FITC tracer in vascular tissues, suggesting that injection of PA LPS into the middle ear cavity may induce changes in vascular permeability. These changes are likely due to inflammation, further elucidating the role of PA endotoxin LPS in the pathogenesis of otitis media. Endotoxin LPS activates signaling pathways such as TLR4 and triggers inflammatory responses (Afroz *et al*., 2022). Furthermore, endotoxin LPS induces pericyte migration and disrupts tight junction structures, leading to dysfunction of pericytes which, in turn, affects vascular function (Castellano *et al*., 2019). Additionally, studies have demonstrated that endotoxin LPS activates perivascular-resident macrophage-like melanocytes, which can regulate tight junction proteins and maintain the integrity of the blood-labyrinth barrier (Urdang *et al*., 2020). This indicates that injection of PA LPS into the middle ear cavity can affect the expression of tight junction-related proteins between endothelial cells in the rat cochlea, thereby impairing the blood barrier.

Conclusion: PA LPS can suppress the biofilm formation of *Candida albicans in vitro*. However, intratumoral injection of PA LPS into the middle ear can cause lymphedema in the cochlea and hearing loss in rats, promoting inflammatory response. In addition, PA LPS can down-regulate the expression of *ZO-1*, *Occludin*, and *VE-cadherin* in the stria vascularis, affecting the function of the blood labyrinth barrier, causing vascular leakage, and destroying the balance of the inner ear. However, a limitation of this study is that it did not directly investigate the mechanism of PA LPS-induced damage to the cochlear structure, nor did it fully clarify the causal relationship between changes in inflammatory factors and hearing loss. Future studies should further explore the direct effects of PA LPS on cochlear tissue and validate the specific mechanisms linking inflammatory factors to hearing loss, thus comprehensively elucidating the role of PA LPS in SOM and its mechanism of disrupting inner ear barrier function.

Declaration of conflicting interests: The author(s) declared no potential conflicts of interest with respect to the research, authorship, and/or publication of this article.

Acknowledgements: We would like to thank all patients for their participation.

Authors' Contribution: Yifei Chen and Jin Nie contributed to the study conception and design. Material preparation, data collection, and analysis were performed by Yifei Chen, Donghai Xie and Jin Nie. The first draft of the manuscript was written by Yifei Chen and Jin Nie, and all authors commented on the previous versions of the manuscript. All authors read and approved the final manuscript.

Funding/Support: There is no Funding/Support.

REFERENCES

Acke, F.R.E., C. De Vriese, H. Van Hoecke and E.M.R. De Leenheer (2022). Twelve years of neonatal hearing screening: audiological and etiological results. Eur. Arch. Otorhinolaryngol., 279(7), 3371–3378. https://doi.org/10.1007/s00405-021-07060-5

Afroz, R., E.M. Tanvir, M. Tania, J. Fu, M.A. Kamal and M.A. Khan (2022). LPS/TLR4 Pathways in breast cancer: insights into cell signalling. Curr. Med. Chem., 29(13), 2274–2289. https://doi.org/10.2174/0929867328666210811145043

Bae, S.H., J.E. Yoo, Y.H. Choe, S.H. Kwak, J.Y. Choi, J. Jung and Y.M. Hyun (2021). Neutrophils infiltrate into the spiral ligament but not the stria vascularis in the cochlea during lipopolysaccharide-induced inflammation. Theranostics, 11(6), 2522–2533. https://doi.org/10.7150/thno.49121

Castellano, G., A. Stasi, R. Franzin, F. Sallustio, C. Divella, A. Spinelli, G. S. Netti, E. Fiaccadori, V. Cantaluppi, A. Crovace, F. Staffieri, L. Lacitignola, G. Grandaliano, S. Simone, G.B. Pertosa and L. Gesualdo (2019). LPS-binding protein modulates acute renal fibrosis by inducing pericyte-to-myofibroblast trans-differentiation through TLR-4 signaling. Int. J. Mol. Sci., 20(15), 3682. https://doi.org/10.3390/ijms20153682

Cayetano, R.D.A., G.B. Kim, J. Park, Y.H. Yang, B.H. Jeon, M. Jang and S.H. Kim (2022). Biofilm formation as a method of improved treatment during anaerobic digestion of organic matter for

biogas recovery. Bioresour. Technol., 344(Pt B), 126309. https://doi.org/10.1016/j.biortech.2021.126309

Chai, Y., W. He, W. Yang, A. P. Hetrick, J. G. Gonzalez, L. Sargsyan, H. Wu, T.T.K. Jung and H. Li (2021). Intratympanic lipopolysaccharide elevates systemic fluorescent gentamicin uptake in the cochlea. Laryngoscope, 131(9), E2573–E2582. https://doi.org/10.1002/lary.29610

Covelli, E., V. Margani, G. Trasimeni, C. Filippi, G. Bandiera, S. Monini and M. Barbara (2022). A case of cavernous hemangioma of the infratemporal fossa causing recurrent secretory otitis media. Braz. J. Otorhinolaryngol., 88(6), 999–1002. https://doi.org/10.1016/j.bjorl.2021.03.001

Cruickshank, D., D.E. Hamilton, I. Iloba and G.S. Jensen (2024). Secreted metabolites from *Pseudomonas*, *Staphylococcus*, and *Borrelia* Biofilm: modulation of immunogenicity by a nutraceutical enzyme and botanical blend. Microorganisms, 12(5), 991. https://doi.org/10.3390/microorganisms12050991

Delaney, D.S., L.J. Liew, J. Lye, M.D. Atlas and E.Y.M. Wong (2023). Overcoming barriers: a review on innovations in drug delivery to the middle and inner ear. Front. Pharmacol., 14, 1207141. https://doi.org/10.3389/fphar.2023.1207141

Du, J., G. Yin, Y. Hu, S. Shi, J. Jiang, X. Song, Z. Zhang, Z. Wei, C. Tang and H. Lyu (2020). Coicis semen protects against focal cerebral ischemia-reperfusion injury by inhibiting oxidative stress and promoting angiogenesis via the TGFβ/ALK1/Smad1/5 signaling pathway. Aging, 13(1), 877–893. https://doi.org/10.18632/aging.202194

Glueckert, R., L. Johnson Chacko, H. Rask-Andersen, W. Liu, S. Handschuh and A. Schrott-Fischer (2018). Anatomical basis of drug delivery to the inner ear. Hear. Res., 368, 10–27. https://doi.org/10.1016/j.heares.2018.06.017

Gu, J., L. Tong, X. Lin, Y. Chen, H. Wu, X. Wang and D. Yu (2022). The disruption and hyperpermeability of blood-labyrinth barrier mediates cisplatin-induced ototoxicity. Toxicol. Lett., 354, 56–64. https://doi.org/10.1016/j.toxlet.2021.10.015

Hu, Y., H. Dong, J. Huang, J. Huang, D. Tao, C. Huang, L. Hu, H. Xu and Y. Sun (2021). Long non-coding RNA (lncRNA) nuclear enriched abundant transcript 1 (NEAT1) promotes the inflammation and apoptosis of otitis media with effusion through targeting microRNA (miR)-495 and activation of p38 MAPK signaling pathway. Bioengineered, 12(1), 8080–8088. https://doi.org/10.1080/21655979.2021.1982842

Haas, A.J., C. Zihni, S.M. Krug, R. Maraspini, T. Otani, M. Furuse, A. Honigmann, M.S. Balda and K. Matter (2022). *ZO-1* guides tight junction assembly and epithelial morphogenesis via cytoskeletal tension-dependent and -independent functions. Cells, 11(23), 3775. https://doi.org/10.3390/cells11233775

Isom, C.M., B. Fort and G.G. Anderson (2022). Evaluating metabolic pathways and biofilm formation in Stenotrophomonas maltophilia. J Bacteriol, 204(1), e0039821. https://doi.org/10.1128/JB.00398-21

Jiang, Y., J. Zhang, Y. Rao, J. Chen, K. Chen and Y. Tang (2019). Lipopolysaccharide disrupts the cochlear blood-labyrinth barrier by activating perivascular resident macrophages and up-regulating MMP-9. Int. J. Pediatr. Otorhinolaryngol., 127, 109656. https://doi.org/10.1016/j.ijporl.2019.109656

Kim, B.G., D.Y. Choi, M.G. Kim, A.S. Jang, M.W. Suh, J.H. Lee, S.H. Oh and M.K. Park (2022). Effect of angiogenesis and lymphangiogenesis in diesel exhaust particles inhalation in mouse model of LPS induced acute otitis media. Front. Cell. Infect. Microbiol., 12, 824575. https://doi.org/10.3389/fcimb.2022.824575

Ko, Y.S., E.J. Gi, S. Lee and H.H. Cho (2023). Dual red and near-infrared light-emitting diode irradiation ameliorates LPS-induced otitis media in a rat model. Front. Bioeng. Biotechnol., 11, 1099574. https://doi.org/10.3389/fbioe.2023.1099574

Kaya, Z., M. Yayla, I. Cinar, N. E. Atila, S. Ozmen, Z. Bayraktutan and D. Bilici (2019). Epigallocatechin-3-gallate (EGCG) exert therapeutic effect on acute inflammatory otitis media in rats. Int. J. Pediatr. Otorhinolaryngol., 124, 106–110. https://doi.org/10.1016/j.ijporl.2019.05.012

Li, E., S. Li, S. Wang, Q. Li, D. Pang, Q. Yang, Q. Zhu and Y. Zou (2023). Antibacterial effects of Ramulus mori oligosaccharides against Streptococcus mutans. Foods, 12(17), 3182. https://doi.org/10.3390/foods12173182

Lechien, J.R., S. Hans, F. Simon, M. Horoi, C. Calvo-Henriquez, C.M. Chiesa-Estomba, M. Mayo-Yáñez, R. Bartel, K. Piersiala, Y. Nguyen and S. Saussez (2021). Association between laryngopharyngeal reflux and media otitis: a systematic review. Otol. Neurotol., 42(7), e801–e814. https://doi.org/10.1097/MAO.0000000000003123

Lin, H.W., T.C. Chen, J.H. Yeh, S.C. Tsou, I. Wang, T.J. Shen, C.J. Chuang and Y.Y. Chang (2022).

Suppressive effect of tetrahydrocurcumin on *Pseudomonas aeruginosa* lipopolysaccharide-induced inflammation by suppressing JAK/STAT and Nrf2/HO-1 pathways in microglial cells. Oxid. Med. Cell Longev., 2022, 4978556. https://doi.org/10.1155/2022/4978556

Lin, Y.C., C.P. Shih, H.C. Chen, Y.L. Chou, H.K. Sytwu, M.C. Fang, Y.Y. Lin, C.Y. Kuo, H.H. Su, C.L. Hung, H.K. Chen and C.H. Wang (2021). Ultrasound microbubble-facilitated inner ear delivery of gold nanoparticles involves transient disruption of the tight junction barrier in the round window membrane. Front. Pharmacol., 12, 689032. https://doi.org/10.3389/fphar.2021.689032

Liu, J., R. Kang and D. Tang (2024). Lipopolysaccharide delivery systems in innate immunity. Trends Immunol., 45(4), 274–287. https://doi.org/10.1016/j.it.2024.02.003

Offor, B.C., M.I. Mhlongo, P.A. Steenkamp, I.A. Dubery and L.A. Piater (2022). Untargeted metabolomics profiling of arabidopsis WT, lbr-2-2 and bak1-4 mutants following treatment with two LPS chemotypes. Metabolites, 12(5), 379. https://doi.org/10.3390/metabo12050379

Oliveras-Cañellas, N., J. Latorre, E. Santos-González, A. Lluch, F. Ortega, J. Mayneris-Perxachs, J.M. Fernández-Real and J.M. Moreno-Navarrete (2023). Inflammatory response to bacterial lipopolysaccharide drives iron accumulation in human adipocytes. Biomed. Pharmacother., 166, 115428. https://doi.org/10.1016/j.biopha.2023.115428

Pereira, R., R.O. Dos Santos Fontenelle, E.H.S. de Brito and S.M. de Morais (2021). Biofilm of *Candida albicans*: formation, regulation and resistance. J. Appl. Microbiol., 131(1), 11–22. https://doi.org/10.1111/jam.14949

Pang, K., Y. Di, G. Li, J. Li, X. Li and L. Sun (2020). Can reflux symptom index and reflux finding score be used to guide the treatment of secretory otitis media in adults? ORL. J. Otorhinolaryngol. Relat. Spec., 82(3), 130–138. https://doi.org/10.1159/000505929

Bai, Y., M. Hu, F. Ma, K. Liu, H. Xu, X. Wu and H. Wang (2021). Self-Reported Allergic Rhinitis Prevalence and Related Factors in Civil Aviation Aircrew of China. Aerosp. Med. Hum. Perform., 92(1), 25–31. https://doi.org/10.3357/AMHP.5727.2021

Rawat, M., M. Nighot, R. Al-Sadi, Y. Gupta, D. Viszwapriya, G. Yochum, W. Koltun and T.Y. Ma (2020). IL1B increases intestinal tight junction permeability by up-regulation of MIR200C-3p, which degrades *occludin* mRNA. Gastroenterology, 159(4), 1375–1389. https://doi.org/10.1053/j.gastro.2020.06.038

Runge, A., S. Straif, Z. Banki, W. Borena, B. Muellauer, J. Brunner, T. Gottfried, J. Schmutzhard, J. Dudas, B. Risslegger, A. Randhawa, C. Lass-Flörl, D. von Laer and H. Riechelmann (2023). Viral infection in chronic otitis media with effusion in children. Front. Pediatr. 11, 1124567. https://doi.org/10.3389/fped.2023.1124567.

Sekulic-Jablanovic, M., J. Paproth, C. Sgambato, G. Albano, D.G. Fuster, D. Bodmer and V. Petkovic (2022). Lack of NHE6 and inhibition of nkcc1 associated with increased permeability in blood labyrinth barrier-derived endothelial cell layer. Front. Cell Neurosci. 16, 862119. https://doi.org/10.3389/fncel.2022.862119

Sung, C.Y.W., N. Hayase, P.S.T. Yuen, J. Lee, K. Fernandez, X. Hu, H. Cheng, R.A. Star, M.E. Warchol and L.L. Cunningham (2023). Macrophage depletion protects against cisplatin-induced ototoxicity and nephrotoxicity. Sci. Adv., 10(30), eadk9878. https://doi.org/10.1101/2023.11.16.567274

Urdang, Z.D., J.L. Bills, D.Y. Cahana, L.L. Muldoon and E.A. Neuwelt (2020). Toll-like receptor 4 signaling and downstream neutrophilic inflammation mediate endotoxemia-enhanced blood-labyrinth barrier trafficking. Otol. Neurotol., 41(1), 123–132. https://doi.org/10.1097/MAO.0000000000002447

Weiss, B.G., S. Freytag, B. Kloos, F. Haubner, K. Sharaf, J.L. Spiegel, M. Canis, F. Ihler and M. Bertlich (2021). Cannabinoid receptor 2 agonism is capable of preventing lipopolysaccharide induced decreases of cochlear microcirculation - a potential approach for inner ear pathologies. Otol. Neurotol., 42(9), e1396–e1401. https://doi.org/10.1097/MAO.0000000000003280

Wang, S., D. Xiang, F. Tian and M. Ni (2021). Lipopolysaccharide from biofilm-forming *Pseudomonas aeruginosa* PAO1 induces macrophage hyperinflammatory responses. J. Med. Microbiol. 70(4), 001352. https://doi.org/10.1099/jmm.0.001352

Yang, D., W. Yan, J. Qiu, Y. Huang, T. Li, Y. Wang, N. Wang, C. Durkan, J. Huang, T. Yin and G. Wang (2020). Mussel adhesive protein fused with *VE-cadherin* extracellular domain promotes endothelial-cell tight junctions and in vivo endothelization recovery of vascular stent. J. Biomed. Mater. Res. B. Appl. Biomater. 108(1), 94–103. https://doi.org/10.1002/jbm.b.34369

Yang, Z., Z. Zhang, J. Zhu, Y. Ma, J. Wang and J. Liu (2022). Analysis of the plasmid-based *ts* allele

of *PA0006* reveals its function in regulation of cell morphology and biosynthesis of core lipopolysaccharide in *Pseudomonas aeruginosa*. Appl. Environ. Microbiol., 88(14), e0048022. https://doi.org/10.1128/aem.00480-22

Zhang, Y.N., M. Bai, X.X. Hui, S. Wang and M.S. Miao (2021). Animal model analysis of secretory otitis media based on characteristics of clinical symptoms of traditional Chinese and Western medicine. Zhongguo Zhong Yao Za Zhi, 46(4), 767–771. https://doi.org/10.19540/j.cnki.cjcmm.20201113.601

Zhang, N., T. Qian, S. Sun, W. Cao, Z. Wang, D. Liu, P. Li, J. Wu, H. Li and J. Yang (2022). IL-17 is a potential therapeutic target in a rodent model of otitis media with effusion. J. Inflamm. Res., 15, 635–648. https://doi.org/10.2147/JIR.S338598

Zheng, J., A. Gu, L. Kong, W. Lu, J. Xia, H. Hu and M. Hong (2024). Cimifugin relieves histamine-independent itch in atopic dermatitis via targeting the CQ receptor MrgprA3. ACS Omega, 9(6), 7239–7248. https://doi.org/10.1021/acsomega.3c09697.